Neutron single-particle strengths at N=40, 42: Neutron knockout from ^{68,70}Ni ground and isomeric states

F. Recchia *et al.*

Neutron single-particle strengths at $N = 40, 42$: Neutron knockout from ^{68,70}Ni ground and isomeric states

F. Recchia,[1, 2, *] D. Weisshaar,[1] A. Gade,[1, 3] J. A. Tostevin,[4] R. V. F. Janssens,[5] M. Albers,[5]
V. M. Bader,[1, 3] T. Baugher,[1, 3, †] D. Bazin,[1] J. S. Berryman,[1] B. A. Brown,[1, 3] C. M. Campbell,[6]
M. P. Carpenter,[5] J. Chen,[7, ‡] C. J. Chiara,[5, §] H. L. Crawford,[6] C. R. Hoffman,[5] F. G. Kondev,[7]
A. Korichi,[5, 8] C. Langer,[1] T. Lauritsen,[5] S. N. Liddick,[1, 9] E. Lunderberg,[1, 3] S. Noji,[1]
C. Prokop,[1, 9] S. R. Stroberg,[1, 3, ¶] S. Suchyta,[1, 9, **] K. Wimmer,[1, 10, ††] and S. Zhu[5]

[1] *National Superconducting Cyclotron Laboratory, Michigan State University, East Lansing, Michigan 48824, USA.*
[2] *Dipartimento di Fisica e Astronomia "Galileo Galilei",*
Università degli Studi di Padova and INFN Padova, I-35131 Padova, Italy.
[3] *Department of Physics and Astronomy, Michigan State University, East Lansing, Michigan 48824, USA.*
[4] *Department of Physics, University of Surrey, Guildford, Surrey GU2 7XH, United Kingdom.*
[5] *Physics Division, Argonne National Laboratory, Argonne, Illinois 60439, USA.*
[6] *Nuclear Science Division, Lawrence Berkeley National Laboratory, Berkeley, California 94720, USA.*
[7] *Nuclear Engineering Division, Argonne National Laboratory, Argonne, Illinois 60439, USA.*
[8] *CSNSM-IN2P3/CNRS, F-91405 Orsay Campus, France.*
[9] *Department of Chemistry, Michigan State University, East Lansing, Michigan 48824, USA.*
[10] *Department of Physics, Central Michigan University, Mt. Pleasant, Michigan 48859, USA.*
(Dated: October 24, 2016)

The distribution of single-particle strength in ^{67,69}Ni was characterized with one-neutron knockout reactions from intermediate-energy ^{68,70}Ni secondary beams, selectively populating neutron-hole configurations at $N = 39$ and 41, respectively. The spectroscopic strengths deduced from the measured partial cross sections to the individual final states, as tagged by their γ-ray decays, are used to identify and quantify neutron configurations in the wave functions. While ^{69}Ni compares well to shell-model predictions, the results for ^{67}Ni challenge the validity of current effective shell-model Hamiltonians by revealing discrepancies that cannot be explained so far. These results suggest that our understanding of the low-lying states in the neutron-rich, semi-magic Ni isotopes may be incomplete and requires further investigation on both the experimental and theoretical sides.

PACS numbers: 23.20.Lv, 21.10.Tg, 21.60.Cs, 27.50.+e

I. INTRODUCTION

The nuclei around neutron-rich ^{68}Ni have attracted much attention in recent years. They present a case of coexisting prolate, oblate and spherical 0^+ states below 2.6 MeV excitation energy in a region of the nuclear chart where shell evolution is at play [1–3]. This region represents a challenging testing ground for nuclear structure models that attempt to incorporate the driving forces of structural change to reliably predict the properties of medium-heavy nuclei also at large isospin.

Configuration-interaction shell-model approaches have been among the most successful to describe a wide range of properties of medium-heavy nuclei. Shell gaps are important as they demark the model spaces and the assumed inert cores of closed-shell configurations. As nucleons are added to a closed shell, correlation effects drive the shape of the nucleus away from sphericity; i.e., to oblate and prolate deformation. A critical ingredient for benchmarking and improving the effective interactions that underlie configuration-interaction models is experimental information that characterizes the relevant degrees of freedom, specifically the single-particle structure. Often, systematic trends and striking differences between neighboring isotopes and isotones shed light on aspects of the underlying nuclear interactions that need to be understood.

The spin-isospin parts of the nucleon-nucleon interaction; e.g., the proton-neutron tensor force (in particular, the strongly attractive monopole parts), are known to modify shell structure in exotic nuclei [4–6]. In some neutron-rich regions of the nuclear chart, the magic numbers established in the valley of stability break down and new shell gaps can emerge [7, 8]. New regions of deformation appear which can be attributed to the promotion of nucleons to high-j orbitals located just above a shell closure [9]. These changes to the intrinsic shell structure are

* e-mail: francesco.recchia@unipd.it
† Present address: Los Alamos National Laboratory, Los Alamos, New Mexico 87545, USA.
‡ Present address: National Superconducting Cyclotron Laboratory, Michigan State University, East Lansing, Michigan 48824, USA.
§ Present address: U.S. Army Research Laboratory, Adelphi, Maryland 20783, USA.
¶ Present address: TRIUMF, Vancouver, British Columbia V6T 2A3, Canada.
** Present address: Department of Nuclear Engineering, University of California Berkeley, Berkeley, California 94720, USA.
†† Present address: Department of Physics, The University of Tokyo, Hongo, Bunkyo-ku, Tokyo 113-0033, Japan.

of fundamental interest, but also have implications for r-process nucleosynthesis. For example, in the Ni isotopic chain, they directly affect the role of ^{78}Ni as a waiting point nucleus [10].

As recently highlighted [2], shell evolution can operate within a single nucleus: deformation-driving two- and multi-particle-hole configurations can compete with spherical ones, resulting in two or more coexisting structures at low excitation energy in the same nucleus. Of particular interest is the region around the proton magic ($Z = 28$) ^{68}Ni where the $N = 40$ harmonic-oscillator shell gap separates the fp and the $g_{9/2}$ neutron orbitals. The first excited state of ^{68}Ni, a 0_2^+ level at 1604 keV [1, 11], hints at the possibility of shape coexistence at low excitation energy. Other evidence comes from the existence of a low-lying 0_3^+ state and from the observed decay patterns of the associated 2^+ states [11, 12]. All of these experimental observations, in agreement with theoretical predictions by Tsunoda *et al.* [2], point to a rather peculiar structure for this nucleus where spherical, oblate- and prolate-shaped structures coexist in a narrow energy range, differing in binding energy by at most 2.51 MeV.

As protons are removed from ^{68}Ni, a region of deformation centered on ^{64}Cr develops [13–18], where the main components of the ground-state wave function are dominated by configurations in which neutrons are promoted from the fp shell to the $g_{9/2}$ orbital across the $N = 40$ gap. Adding neutrons to ^{68}Ni, the $Z = 28$ gap is predicted to become smaller when moving from ^{68}Ni to ^{78}Ni, as a result of the attraction between the proton $f_{5/2}$ and the neutron $g_{9/2}$ orbitals and the repulsion between the proton $f_{7/2}$ and neutron $g_{9/2}$ configurations. This leads to deformation that may enhance specific configurations, for instance those that are characterized by a higher neutron occupancy of the $g_{9/2}$ and $d_{5/2}$ orbitals. Recent relevant information on $^{67-70}$Ni stems from a number of measurements using a wide variety of experimental techniques, such as β decay, deep-inelastic reactions, searches for isomeric states and transfer reactions [1, 11, 12, 19–25].

In this region of rapid structural change and shape coexistence, the neutron single-particle structure along the Ni isotopic chain is of great interest; as it is important to track: (a) the onset of neutron excitations into the $g_{9/2}$ and $d_{5/2}$ orbitals across the $N = 40$ sub-shell gap, and (b) the difference in configurations between ^{68}Ni and ^{70}Ni. To address these issues, exclusive one-neutron knockout cross sections from intermediate-energy ^{68,70}Ni projectiles were measured using γ-ray tagging of the final state [26]. This technique allows one to identify and quantify neutron configurations in the ^{68}Ni and ^{70}Ni initial states. Specifically, the partial cross sections to the lowest-lying $1/2^-$, $5/2^-$, $3/2^-$ and $9/2^+$ states or candidate states of ^{67,69}Ni are measured and compared to calculations that combine shell-model spectroscopic strengths and eikonal reaction theory. Cross sections were also determined for one-neutron removal from long-lived isomers present in both the ^{68}Ni and ^{70}Ni projectiles. The following sections describe the experiment and discuss the new results on neutron single-particle strengths in the Ni isotopes as $N = 40$ is crossed.

II. EXPERIMENT

The experiment was performed at the Coupled Cyclotron Facility (CCF) at the National Superconducting Cyclotron Laboratory (NSCL) [27]. Secondary beams of ^{68,70}Ni were produced by fragmentation of a 140 MeV/u ^{82}Se primary beam on a 423-mg/cm^2 ^{9}Be production target located at the entrance of the A1900 separator [28]. The secondary beams, selected and purified with the separator, were delivered at momentum acceptances of 1% for ^{68}Ni and 3% for ^{70}Ni, respectively. In the center of GRETINA, the ^{68}Ni and ^{70}Ni beams impinged on ^{9}Be reaction targets (100- and 281-mg/cm^2 thick, respectively) with mid-target energies of 85 and 74 MeV/u. The measurements described below were carried out with GRETINA [29] and the S800 spectrograph [30].

The ^{68}Ni nucleus has two known isomeric states, the 1604-keV 0_2^+ ($\tau = 390$ ns) and the 2849-keV 5^- ($\tau = 1.24$ ms) states that, if produced in the fragmentation process, survive sufficiently long to be transmitted to the reaction target. ^{70}Ni has only one known isomeric state, the 2861-keV 8^+ ($\tau = 335$ ns) level that, if populated, will survive to the experimental end station as well. Accordingly, to interpret the cross sections for the population of individual final states, the isomeric ratio had to be determined for each projectile beam. For this purpose, a stopper was placed in the center of the GRETINA array and the γ-decay radiation from the implanted nuclei was measured over several microseconds. To determine the ^{68}Ni 5^- and ^{70}Ni 8^+ isomeric content, the number of implanted ions was counted with a plastic scintillator upstream of the stopper. The efficiency-corrected yields of the γ-ray cascades depopulating the two isomers were then used to determine the isomeric ratios. These were 39(4)% for the 5^- level in ^{68}Ni and 8(1)% for the 8^+ one in ^{70}Ni. For the ^{68}Ni 0_2^+ state, the isomeric ratio was determined by the measurement of the 511-keV γ rays following positron annihilation of the internal pair formation, the main decay mode of the first excited 0^+ state. Including corrections for internal conversion, this ^{68}Ni 0_2^+ isomeric ratio was determined to be less than 1%.

The ^{67}Ni and ^{69}Ni one-neutron knockout residues, produced upon collision with the ^{9}Be reaction target, were detected and identified on an event-by-event basis using the time-of-flight and energy-loss information measured with the beam line timing detectors and the S800 spectrograph focal-plane detector system [30]. Prompt γ rays, emitted in-flight from the de-excitation of the knockout residues, were detected with the GRETINA array [29] surrounding the target at the entrance of the S800 spectrograph. The γ-ray energies were Doppler corrected on an event-by-event basis using the reconstructed momen-

tum vector provided by the S800 spectrograph for each reaction residue [30]. The Doppler-reconstructed spectra of ^{67,69}Ni are displayed in Figs. 1 and 2.
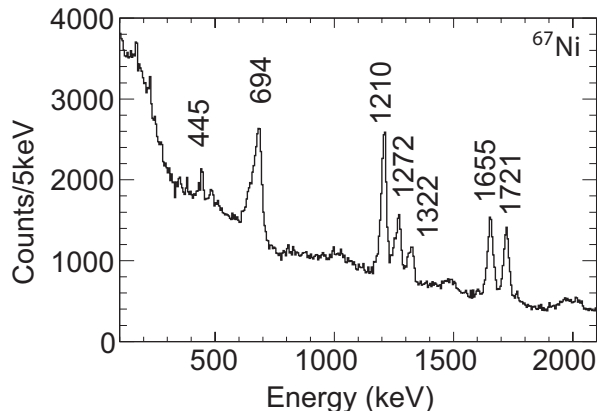

FIG. 1. Doppler-reconstructed γ-ray spectrum detected in coincidence with ^{67}Ni. The 694-keV transition is broadened by a lifetime effect of approximately 216 ps [31]. The Doppler reconstruction was performed with a velocity v/c = 0.401.
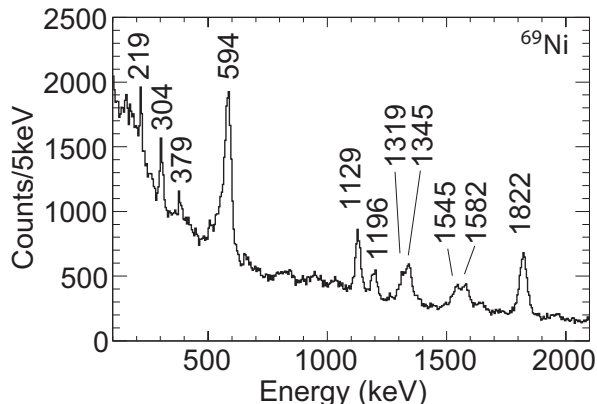

FIG. 2. Doppler-reconstructed γ-ray spectrum detected in coincidence with ^{69}Ni. The 594-keV transition is broadened by a lifetime effect of approximately 170 ps [31]. The Doppler reconstruction was performed with a velocity v/c = 0.371.

The measured inclusive cross sections for the ^{9}Be(^{68}Ni,^{67}Ni)X and ^{9}Be(^{70}Ni,^{69}Ni)X one-neutron removal reactions, σ_{inc}^{-1n} = 133(10) and 168(13) mb, respectively, were derived from the yield of the ^{67,69}Ni reaction residues relative to the number of incoming ^{68,70}Ni projectiles and the number density of the reaction target.

The projectile-like reaction residues, after traversing the trigger plastic scintillator at the back of the S800 focal plane, were implanted into an aluminum plate placed in front of a CsI(Na) detector array [32]. The delayed γ-ray detection with the scintillator array in this IsoTagger configuration [33] enabled measurements of transitions from isomers in the knockout residues.

III. RESULTS AND DISCUSSION

The efficiency-corrected intensities were obtained taking into account the effect of the Lorentz boost for γ-ray distributions emitted in-flight. The intensity for some of the transitions, forming energy doublets or multiplets, had to be obtained using γ-gated coincidence spectra. In ^{67}Ni and ^{69}Ni, the 694-keV and 594 keV transitions are affected by state lifetimes of 216(6) and 173(49) ps, respectively [31]. These lifetimes are long enough to generate a line shape, after Doppler reconstruction, with a characteristic low-energy tail indicative of γ emission behind the target. To determine the intensity of these transitions, Monte Carlo simulations, based on the AGATA simulation package [34] modified for the GRETINA geometry [35], were used. The measured intensities for ^{67}Ni and ^{69}Ni are reported in Tables I and II.

The transitions delayed by the 19.2 μs, $9/2^+$ isomer in ^{67}Ni were detected in the CsI(Na) array in the S800 focal plane. The corresponding efficiency was determined with the methods described in Ref. [33]. The consistency of this efficiency was confirmed by exploiting coincidence relationships within delayed γ-ray cascades.

Final-state exclusive cross sections were determined for all states placed in the level scheme: These are reported in Tables III and IV. The cross sections were obtained from the γ-ray intensities relative to the number of knockout residues. The cross section for the direct population of the 1008-keV $9/2^+$ isomer in ^{67}Ni was obtained from the difference between the total intensity of the depopulating delayed transitions, as measured with the CsI(Na) scintillator array, and that of the prompt feeding transitions, as obtained from GRETINA. It was not possible to use the same method for the $1/2^-$ isomer at 321(2) keV in ^{69}Ni as its long half-life of 3.5 s prevented the measurement of implantation-decay correlations with the scintillator array. Thus, the population of the $1/2^-$ isomer in the knockout reaction cannot be distinguished from that of the ground state, as both are characterized through the non-observation of a decay γ ray. The experimen-

TABLE I. Energies and relative intensities of the prompt γ-ray transitions observed in coincidence with ^{67}Ni reaction residues.

^{68}Ni$\rightarrow^{67}$Ni	E_γ(keV)	I_γ (%)
	172(1)	5(2)
	445(1)	6.3(12)
	694(5)	81.2(13)
	1193(4)	11(3)
	1210(4)	100(5)
	1249(5)	20(6)
	1272(2)	27(6)
	1322(4)	29(3)
	1655(1)	63(2)
	1721(2)	58(2)
	1768(4)	7.2(6)

tal partial cross sections were corrected for the measured content of the 0_1^+ ground state and the 5^- isomer in the ^{68}Ni projectile beam, the $\leq 1\%$ isomeric content from the 0_2^+ state is neglected. For the ^{70}Ni projectiles, the 8(1)% of 8^+ isomeric content was corrected for, but in the table only the comparison for the cross sections from the projectile ground state are provided.

The theoretical partial and inclusive cross section calculations follow Refs. [38, 39]. The cross section for neutron removal from an initial state i of the A-body projectile – here its ground or an isomeric state – to a given residue final state f is given by

$$\sigma_\alpha^{fi} = \left(\frac{A}{A-1}\right)^N C^2 S \, \sigma_\alpha^{sp}, \qquad (1)$$

where $C^2 S$ is the shell-model spectroscopic factor and σ_α^{sp} the single-particle cross section. Here, α labels the quantum numbers n, ℓ, j of the removed nucleon. The A-dependent multiplicative term is a center-of-mass correction factor to the shell-model $C^2 S$ value for removal from an orbital with N oscillator quanta [40]. The single-particle cross section σ_α^{sp} is obtained with the eikonal approach [38], assuming a normalized single-particle overlap form factor for the removed nucleon and complex residue- and nucleon-target optical potentials. Full details of the model parameter values, the shell-model spectroscopy and the calculated partial cross sections are presented as Supplemental Material accompanying this publication [37]. The parallel momentum distributions of the knockout residues, in the projectile rest-frame, which reflect the orbital angular momentum ℓ of the initial state

TABLE II. Energies and relative intensities of the prompt γ-ray transitions observed in coincidence with ^{69}Ni reaction residues.

^{70}Ni→^{69}Ni	E_γ(keV)	I_γ (%)
	219(1)	6.1(11)
	304(1)	10.8(22)
	379(2)	3.3(13)
	594(1)	100.0(54)
	602.4(4)	7.5(26)
	1129(2)	32.4(21)
	1196(2)	15.3(29)
	1319(5)	10.3(26)
	1345(2)	16.0(27)
	1545(4)	17.7(26)
	1582(3)	18.8(28)
	1642(3)	8.3(10)
	1822(2)	61.9(23)

Note: The 602.4-keV transition could not be resolved from 594 keV in the present work. The decay branching ratio of the 1517 keV state was taken from Table I (first column) of Liddick *et al.* [45]. When using the values reported by Mueller *et al.* [44], all intensities must be scaled by a factor 1.05 with the exception of the normalizing intensity of the 594 keV line and the intensity of the 602.4 keV line that is scaled by a factor 1.70.

TABLE III. Measured and calculated inclusive and partial knockout cross sections for ^{68}Ni→^{67}Ni one-neutron knockout. The reported partial cross sections take into account the fact that the ^{68}Ni beam was partly in the 5^- isomeric state (see text). The theoretical cross sections do not include the reduction factor of $R_s \approx 0.7$ that would be expected according to systematics [36]. The theoretical inclusive cross sections were calculated from the partial cross sections (details given in the supplement [37]) taking into account the fractions of 61% and 39% for the ground state and 5^- isomer in ^{68}Ni.

J_f^π	E_{exp}(keV)	$\sigma_{th}(0^+)$	$\sigma_{th}(5^-)$	σ_{exp} (mb)
$1/2_1^-$	0	24.0	10.5	$\leq 86(11)$
$5/2_1^-$	694(5)	40.3		18(2)
$9/2_1^+$	1008(3)	7.5	7.3	<9
$3/2_1^-$	1721(2)	40.9		13.7(14)
$11/2_1^+$	2218(5)		4.4	23(4)
$(9/2_1^+)$	2280(4)	3.1	2.9	<7
$13/2_1^+$	2663(3)		3.8	17(2)
$(11/2_2^+)$	3473(6)		4.6	3.7(10)
$(13/2_2^+)$	3540(6)		6.9	10.0(14)
$15/2_1^+$	3912(6)		10.4	7(2)

^{68}Ni→^{67}Ni $\sigma_{inc}^{exp} = 133(10)$ mb $\qquad \sigma_{inc}^{th} = 118$ mb

of the removed nucleon, are calculated with the same interaction and overlap inputs as outlined above, using the formalism of Ref. [41]. These calculated rest-frame distributions were boosted into the laboratory frame for comparisons with the measured ones.

For ^{67}Ni, the measured exclusive parallel momentum distributions were studied for the 694- and 1721-keV levels by tagging the respective γ-ray transitions of the corresponding energy (see Figs. 3 and 4). The theoretical distributions were obtained by folding the eikonal model momentum distributions with the measured momentum spread of the beam after passing through the target. The orbital angular momentum of the removed neutron leading to the 694-keV state is compatible with the $\ell = 3$ value expected for the $f_{5/2}$ orbital, while that observed for the 1721-keV state is best described by removal from an $\ell = 1$ orbital, presumably $p_{3/2}$. These observations confirm the previous spin-parity assignments for these states [20].

Because of the complex feeding of the excited states and of some doublet structures in their decays it was not possible to study the parallel momentum distributions of the knockout residues tagged on the decay from higher-lying states.

For ^{69}Ni, an analysis of the momentum distributions was not possible since, to obtain the required statistics, the measurement was run with a momentum acceptance of 3% for ^{70}Ni, instead of the 1% used for ^{68}Ni. This loss in momentum resolution prohibits the discrimination of different ℓ values in this case.

TABLE IV. Measured and calculated inclusive and partial knockout cross sections for ^{70}Ni→^{69}Ni one-neutron removal assuming the tentative level scheme presented in Fig. 8. The theoretical cross sections do not include the reduction factor of $R_s \approx 0.7$ that would be expected according to systematics [36]. The small theoretical partial cross sections for knockout from the 8^+ isomer are not listed since their contributions are well within the experimental uncertainties (for completeness, all cross sections are available in the supplement). The theoretical inclusive cross sections were calculated from the partial cross sections (details given in the supplement [37]) taking into account both the fractions of 92% and 8% for the ground state and 8^+ isomer in ^{70}Ni.

J_f^π	E_{exp}(keV)	$\sigma_{th}(0^+)$	σ_{exp} (mb)
$9/2^+$	0	24.1	$\left.\begin{array}{c} \\ \end{array}\right\} \leq 83(5)$ *
$1/2^-$	321(2)	21.0	
$5/2^-$	915(3)	25.4	$26(3)^\dagger$
$(1/2^-, 3/2^-)$	1450(3)	$10.4^\#$	8(1)
$5/2^-$	1517(3)	5.7	$6(1)^\dagger$
$(1/2^-, 3/2^-)$	1640(3)	$3.9^\#$	4(1)
$(1/2^-, 3/2^-)$	1866(4)	$12.1^\#$	2(1)
$(3/2^-)$	2143(3)	$13.9^\#$	16(2)
	2170(3)	$1.8^{\,\&}$	2.8(6)

^{70}Ni→^{69}Ni	$\sigma_{inc}^{exp} = 168(13)$ mb		$\sigma_{inc}^{th} = 133$ mb

* Note: It is not possible to separate the cross section attributed to the ground state from the cross section attributed to the long-lived $1/2^-$ isomeric state.
$^\#$ Note: Assuming $J^\pi = 3/2^-$
$^{\&}$ Note: Assuming $J^\pi = 5/2^-$
† Note: The decay branching ratio of the 1517 keV state was taken from Table I (first column) of Liddick *et al.* [45]. Using the branching reported by Mueller *et al.* [44], the partial cross sections are 25(3) and 7(1) mb for the knockout to the 915 and 1517 keV states, respectively.
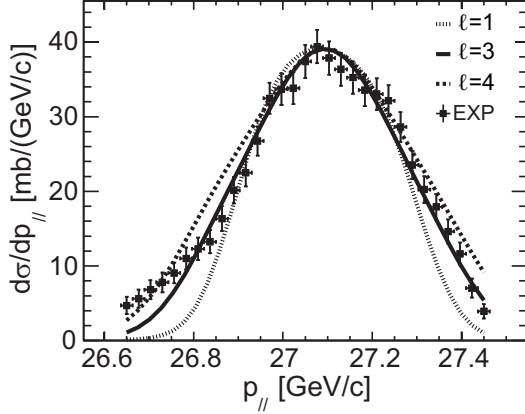

FIG. 3. Measured parallel momentum distribution for the population of the level at 694 keV in ^{67}Ni compared to calculated distributions assuming different ℓ values for the removed neutron. The measured distribution is best reproduced by the removal of a neutron from the $\ell = 3$, $f_{5/2}$ orbital of ^{68}Ni.
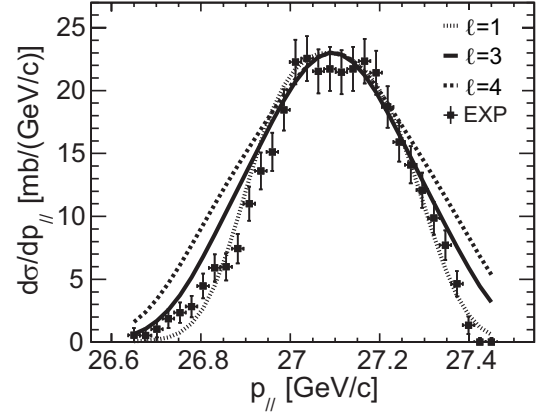

FIG. 4. Parallel momentum distributions of ^{67}Ni knockout residues left in the 1721-keV state. This distribution is best reproduced by an $\ell = 1$ distribution, as expected for neutron removal from the $p_{3/2}$ orbital of ^{68}Ni.

A. ^{67}Ni

Previous studies of ^{67}Ni already identified a number of excited states. Gamma-gamma coincidence relationships, intensity arguments, and comparisons with shell-model predictions were used to construct a level scheme based on the present work (see Fig. 5). Spin-parity assignments are proposed, supported by the study of the parallel momentum distributions for the states whenever possible.

The level scheme of Fig. 5 is in agreement with that obtained from spectroscopy following deep inelastic reactions performed at Argonne National Laboratory [20]. As displayed in Fig. 6, prompt γ-γ coincidence relation-
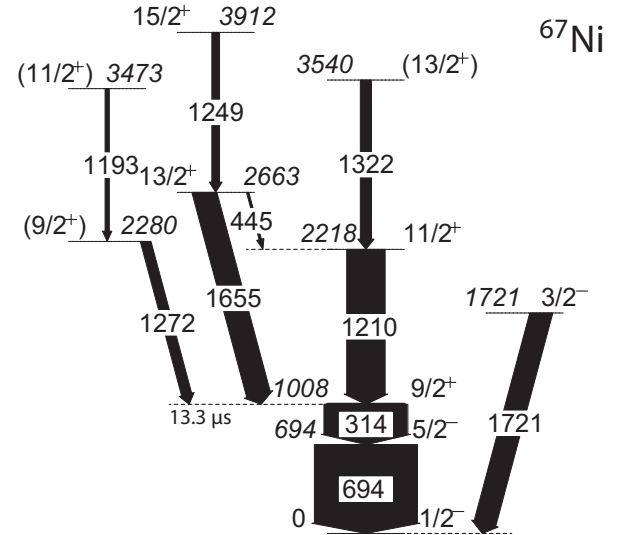

FIG. 5. Proposed level scheme for ^{67}Ni from this work. The widths of the arrows are proportional to the efficiency-corrected γ-ray intensities. The half life of the $9/2^+$ isomer is indicated.
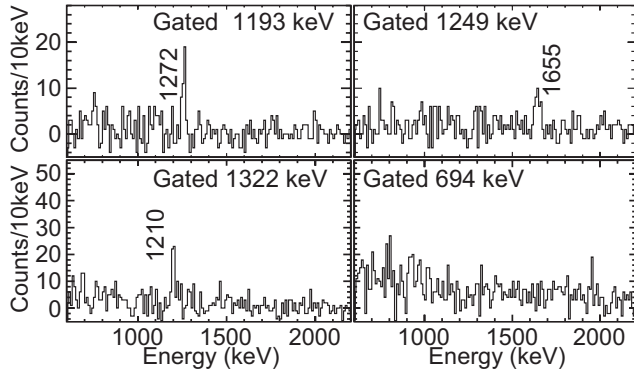
FIG. 6. ^{67}Ni $\gamma\gamma$-ray coincidence spectra. The spectra establish the coincidence relationship between the 1193- and 1272-keV transitions, the 1249- and 1655-keV γ rays and the 1322- and 1210-keV transitions. Note that the spectrum gated on the 694-keV transition does not indicate any prompt coincident feeder.
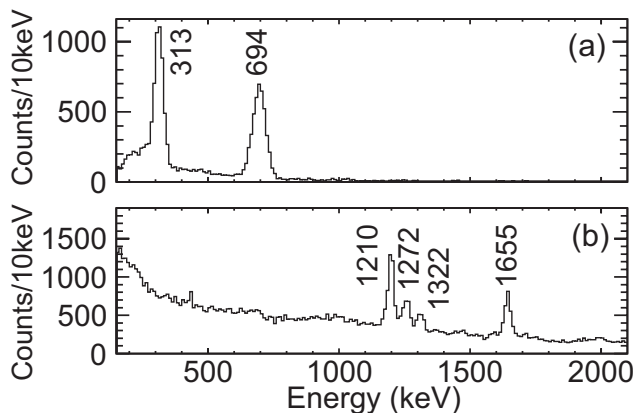

FIG. 7. Spectra of ^{67}Ni taken with (a) the CsI(Na) array and (b) with GRETINA (only prompt events) gated on the 313-keV or the 694-keV delayed transitions retarded by the $9/2^+$ isomer.

ships confirm the 1193-1272 keV and the 1249-1655 keV cascades. In the γ-ray singles spectrum, a 445-keV γ ray is visible that matches the energy difference between the 1655- and 1210-keV γ rays from the 2663- and 2218-keV states, thus supporting the decay pattern proposed by Zhu et al. [20]. As stated above, a 694-keV prompt transition is observed in GRETINA with a line shape indicative of a lifetime compatible with the reported value, $\tau = 216(6)$ ps [31]. The same transition is seen in the delayed spectrum recorded in the CsI(Na) array, see Fig. 7(a), as expected in the presence of feeding by the $9/2^+$ isomer.

A number of new transitions were identified as well that can be placed in the level scheme. For the 1322-keV transition, the coincidence relationship with the 1210-

keV decay was used. The placement of the 1272-keV transition in the level scheme is based on the observation that it appears in the prompt spectrum gated on the delayed transitions cascading from the $9/2^+$ isomer (see Fig. 7(b)). As the 1193-keV line was seen in prompt γ-γ coincidence with the 1272-keV γ ray, it is suggested that these two transitions are in a cascade, feeding the $9/2^+$ isomer directly. The ordering is proposed based on the intensities. The γ-ray singles spectrum displays a strong peak at 1721(2) keV. This transition is not feeding the isomer and no additional prompt transitions were found in coincidence. This, together with the parallel momentum distribution indicating $\ell = 1$ orbital angular momentum, suggests that this transition depopulates the low-lying $3/2^-$ state identified at 1724.3(3) keV by Diriken et al. at ISOLDE [42].

B. ^{69}Ni

The nucleus ^{69}Ni has been previously studied using a number of techniques; i.e., isomeric decay [43], β decay [44, 45] and through a (d, p) reaction on ^{68}Ni [46]. The information gathered in these investigations was used in conjunction with the present data to arrive at the level scheme of Fig. 8. Tentative placements of levels are indicated by dashed lines.

Implanting ^{69}Ni isotopes, after identification with the LISE spectrometer at GANIL, Grzywacz and collaborators [43] observed an excited state at 2701 keV that was identified as a $(17/2^-)$ isomer with a half-life of $0.439(3)$ μs. The yrast and yrare sequences of ^{69}Ni were then identified from the decay of this isomer. In particular, it was possible to observe, for the first time, a $594(1)$-keV line corresponding to the transition between a $5/2^-$ state at $915(1)$ keV and the long-lived $1/2^-$ isomeric level at $321(2)$ keV.

The β decay of ^{69}Co was first investigated by Mueller et al. [44]. A number of excited states were identified and a partial level scheme was proposed based on feeding in β decay, but assuming a $7/2^-$ ground state for ^{69}Co. A more recent study by Liddick et al. [45] demonstrated that, while the ground state has a half-life of $0.18(2)$ s, a second isomeric state is also present in ^{69}Co that β decays to ^{69}Ni with a half-life of $0.75(25)$ s. No excitation energy has been measured for this isomer and a tentative $(1/2^-)$ spin-parity assignment was given.

A comprehensive analysis of the γ-decay-tagged β-decay half-life was performed by Liddick et al., comparing the decay curves of γ rays from the β decay of ^{69}Co where: (i) ^{69}Co was directly implanted, and (ii) ^{69}Co was produced as the decay daughter of implanted ^{69}Fe [45]. The much larger relative intensities observed in Ref. [45] for the γ rays at 1129 and 1319 keV relative to the 594-keV transition in the decay chain ^{69}Fe$\rightarrow$^{69}Co$\rightarrow$^{69}Ni with respect to the ^{69}Co$\rightarrow$^{69}Ni one imply that these transitions, most likely, depopulate low spin states. The two transitions are observed in the present experiment without

identification of feeding transitions in coincidence with them. This suggests that the levels depopulated by these γ rays are fed directly in the knockout reaction with little indirect feeding. These transitions are tentatively placed as directly feeding the $1/2^-$ isomer and the proposed tentative J^π assignments are limited to $(1/2^-, 3/2^-)$ for both.

Comparing the transitions observed in Refs. [44] and [45] indicates that the 1545-keV γ ray must be associated (mainly) with the parent state responsible for the 1129- and 1319-keV transitions; e.g., the $(1/2^-)$ isomer in ^{69}Co reported in [45]. Consequently, the corresponding state is tentatively placed above the long-lived 321-keV state in ^{69}Ni. From that, and also on the basis of comparisons with shell-model calculations, it is tentatively assigned as $J^\pi = (1/2^-, 3/2^-)$.

A 304-keV transition is seen in the present data and is established to be in coincidence with the 1545-keV γ ray, but not with the 1196-keV line (Fig. 9). A transition of 304 keV is also reported in Ref. [44], but the available data from the present measurement lead to the conclusion that the γ ray seen here is not the same as that reported in Ref. [44] as there is no indication of the 1821-keV state reported by Mueller *et al.* Hence, based on the coincidence relationships, the 304-1545-keV cascade is proposed to feed directly the 321-keV isomer with the ordering reflecting the measured intensities. This establishes a 2170-keV state with the possible $J^\pi = 1/2^-$, $3/2^-$ or $5/2^-$ quantum numbers reflecting the direct population in the neutron removal reaction.

Using prompt-delayed coincidence events between GRETINA and the CsI(Na) scintillator array, it was possible to establish that the 379-keV transition feeds the $(17/2^-)$ isomer. Being the strongest line in coincidence with the delayed cascade from this $(17/2^-)$ state, it is placed just above the isomer, feeding it directly. Moreover, this transition was not reported in β decay, as one would expect given its placement in the level scheme (Fig. 8). This transition is most certainly populated only by knockout from the 8^+ isomer of ^{70}Ni present with an $8(1)\%$ isomeric ratio in the projectile beam.

A strong transition is observed at 1822 keV, also not reported in β-decay or isomeric-decay experiments. On the basis of systematics, and of its similarity with the 1721-keV state in ^{67}Ni, a $(3/2^-)$ spin-parity is tentatively suggested for the 2143-keV state that then would carry the largest part of the $p_{3/2}$ strength. Finally, a 843-keV transition was observed in the prompt GRETINA spectrum after gating on the delayed transitions depopulating the $(17/2^-)$ isomer. However, such a transition is not observed in the singles spectra and so it is only placed tentatively (dashed line) in the level scheme as directly feeding the high-spin isomer.

C. Discussion

The measured cross sections are compared with the calculations in Figs. 10 and 11 as well as Tables III and IV. The cross section to the ground state is obtained by subtracting those to all excited states from the inclusive cross section. This implies that all unobserved direct feeding to the ground state or to long-lived isomeric states is included in the ground-state cross section, making its value an upper limit. The calculations presented here make use of shell-model spectroscopic factors. Shell-model (SM) calculations, including only neutron configurations in the $f_{5/2}pg_{9/2}$ valence space were performed with the code NuShellX [47] assuming a ^{56}Ni core and the jj44pna [48] effective interaction.

For both ^{68}Ni and ^{70}Ni, relevant strength was identified to $1/2^-$, $5/2^-$, $9/2^+$, and $3/2^-$ candidate states, corresponding to neutron removal from the $p_{1/2}$, $f_{5/2}$, $g_{9/2}$ and $p_{3/2}$ orbitals close to the Fermi surface. Several problems arise, however, in detailed quantitative comparisons. First, based on the calculated effective neutron-proton Fermi-surface asymmetries, $\Delta S \approx -6$ to -9 MeV (quoted in the supplementary material [37]) the experimental and theoretical inclusive cross sections would be expected to differ by a reduction factor, $R_s = \sigma^{exp}/\sigma^{th}$, of order 0.7, based on removal reaction systematics [36]. That is, usually, the shell- plus eikonal models overestimate the cross section (and the total spectroscopic strength) leading to bound final states. This usual reduction is not observed in the cross section comparisons of Tables III and IV and Figs. 10 and 11. However, this observation might be expected considering the shell-model orbitals used here, which, so far, neglect possible neutron $f_{7/2}$ single-particle strength leading to ^{67}Ni and ^{69}Ni final states below their first neutron thresholds of 5.808(3) and 4.586(5) MeV, respectively.

Such neutron $f_{7/2}$ removal strength is not included in the calculated inclusive cross sections of Tables III and IV. The positions of the neutron $f_{7/2}$ single-particle energies in ^{68,70}Ni, and the associated $f_{7/2}$ strength distributions in ^{67,69}Ni are uncertain, however pf-shell SM calculations suggest that a large fraction of the $f_{7/2}$ strength may populate states below the first neutron thresholds, given above. The calculated single-particle cross section, σ_α^{sp}, for neutron removal to a $7/2^-$ state at the ^{67}Ni(^{69}Ni) threshold, with effective neutron separation energy of 13.6 (11.9) MeV, is 7.32 (7.53) mb. So, the calculated inclusive removal cross sections of Tables III and IV are expected to be underestimated by roughly $N(f_{7/2})\sigma_\alpha^{sp}$, where $N(f_{7/2})$ is the sum of the SM $f_{7/2}$ C^2S spectroscopic factors to bound final states. The unaccounted for $f_{7/2}$ strength would only reconcile the ratio of the experimental and theoretical cross sections with the reduction factor systematics if all of the naive $f_{7/2}$ independent-particle model strength was bound; i.e., $N(f_{7/2}) = 8$. As a rough estimate, fp-shell SM calculations predict $N(f_{7/2}) = 4 - 5.2$ up to $S_n(^{67}\text{Ni}) \pm 1$ MeV.
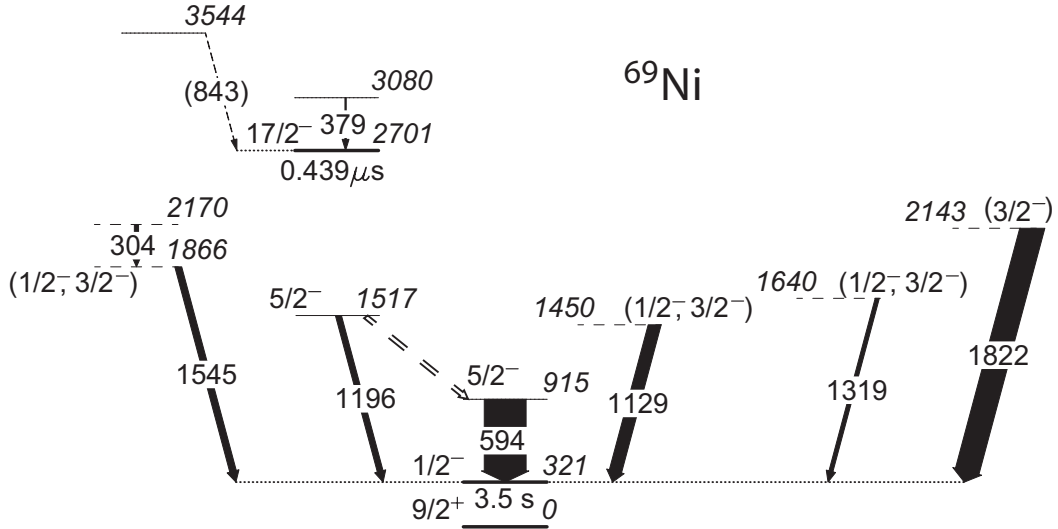
FIG. 8. Proposed level scheme for ^{69}Ni from this work. The widths of the arrows are proportional to the efficiency-corrected γ-ray intensities. The half life of the $1/2^-$ isomer is indicated. Dashed lines indicate levels that are based on our tentative placement of transitions feeding the $1/2^-$ isomer and comparison to shell model (see text). The known transition connecting the levels at 1517 and 915 keV could not be resolved from the 594-keV line in the present work.
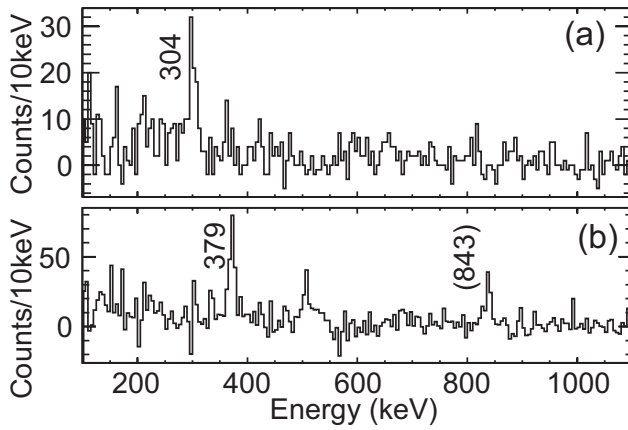

FIG. 9. Coincidence spectra obtained for ^{69}Ni: (a) Prompt γ-γ coincidence between 1545- and 304-keV lines in ^{69}Ni. (b) Prompt spectrum as observed in coincidence with delayed transitions.

FIG. 10. Comparison of measured and calculated cross sections for the reaction ^{68}Ni$\rightarrow^{67}$Ni. Error bars are shown for the experimental data. The triangles mark the upper limits.

Furthermore, for the ^{68}Ni$\rightarrow^{67}$Ni reaction, the following applies: (i) a systematic over-prediction of the cross sections to the low-spin, negative-parity states ($1/2^-$ – $5/2^-$), populated in removal from the ground state of ^{68}Ni, and (ii) a systematic underestimation of the cross sections to high-spin states ($9/2^+$ – $15/2^+$) populated by the removal from the 5^- isomer of ^{68}Ni. The comparison of measured and predicted cross sections for ^{67}Ni relies on the isomeric content in the projectile beam. An 80% 5^- isomeric content for incoming ^{68}Ni (instead of the measured 39(4)%) would be required to explain the relative trend in spectroscopic strength to lower- and higher-spin states exhibited by the data. Given the prevalence of iso-
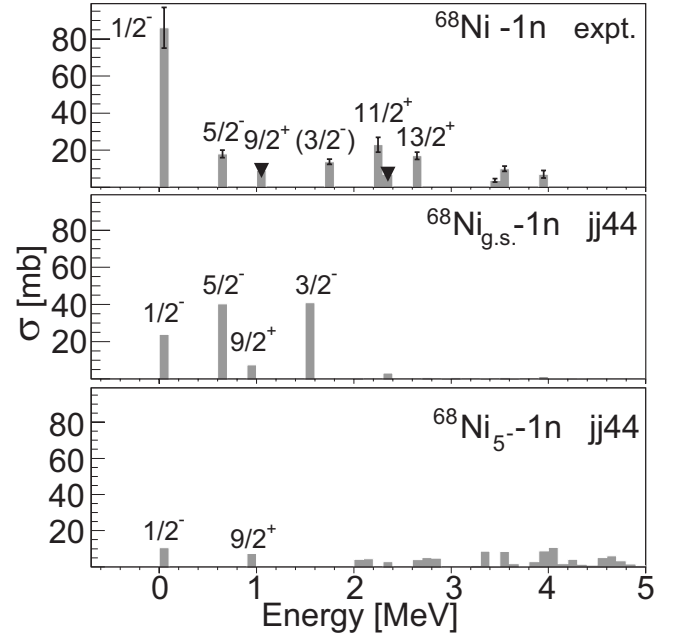
mers in the region, one might consider the possibility of an as yet unobserved isomeric state in ^{68}Ni that would populate higher-spin rather than low-spin states in the knockout reaction. Scenarios of isomeric negative-parity spin 4, 5, 6, 7 and positive-parity spin 5, 6, and 7 states in a lifetime range such that these could have been missed by the isomeric-ratio measurement are unlikely as their placement in energy would have to be rather fine-tuned
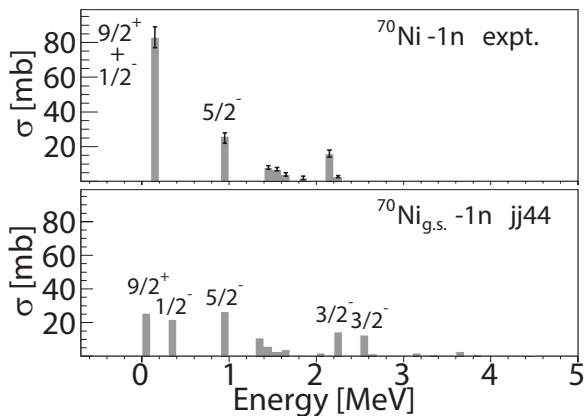
FIG. 11. Comparison of measured and calculated cross sections for the reaction ^{70}Ni$\rightarrow^{69}$Ni. Error bars are shown for the experimental data.

to hinder their prompt decay through the $E^{2\lambda+1}$ suppression of the transitions. Also, SM calculations do not predict such a scenario that would lead to isomers beyond those already observed for ^{68}Ni. Furthermore, the existing body of data for ^{68}Ni is extensive and also provides no indication of isomers beyond the ones observed thus far [1, 11, 12, 21, 22].

One may rather speculate that the discrepancy reported here points to an opportunity to improve the neutron configurations in the SM framework. Table V shows for both cases and initial states the summed theoretical cross sections for the one-neutron knockout from the $p_{1/2}$, $p_{3/2}$, $f_{5/2}$ and $g_{9/2}$ orbitals. While the data for the one-neutron knockout from ^{70}Ni, based on our tentative level scheme and spin assignments, is broadly consistent with the calculations, see Fig. 11, the cross sections to the lowest-lying $3/2_1^-$ and $5/2_1^-$ states are over-predicted for ^{68}Ni $\rightarrow$ ^{67}Ni by a factor of two or more (Table III and Fig. 10). A Hamiltonian with additional mixing could redistribute neutron spectroscopic strengths from these two orbitals into the $g_{9/2}$ level or beyond, for example. However, there is not much room for missing strength associated with the $g_{9/2}$ orbital alone. For comparison, available Hamiltonians, jj44pna (used here), jj44pnb [49], and JUN45 [50] are consistent within less than 15% for the $C^2S(5/2_1^-)$ and $C^2S(3/2_1^-)$ spectroscopic factors. Any improvement to the Hamiltonians in this region would have to preserve the good description of the spectroscopic strength distribution in the knockout to ^{69}Ni.

IV. SUMMARY

Intermediate-energy one-neutron knockout reactions were used to probe the evolution of single-particle structure in the neutron-rich nickel isotopes ^{68}Ni and ^{70}Ni.

The new data enabled the identification of a number of new states in both ^{67}Ni and ^{69}Ni, in particular, levels that carry large parts of the single-particle strength

TABLE V. Calculated cross sections for the orbitals of the active neutron model space within the jj44pna effective interaction for one-neutron knockout from ^{68}Ni and ^{70}Ni for both possible initial states (see Supplemental Material).

| Orbital | ^{68}Ni-1n | | ^{70}Ni-1n | |
	$\sigma_{0_1^+}$ (mb)	σ_{5^-} (mb)	$\sigma_{0_1^+}$ (mb)	σ_{8^+} (mb)
$2p_{1/2}$	24.51	12.70	24.08	24.61
$2p_{3/2}$	42.43	40.22	42.47	11.56
$1f_{5/2}$	41.56	43.58	38.62	34.16
$1g_{9/2}$	12.94	15.46	30.92	25.01
total	121.43	111.96	136.10	95.34

of the neutron orbitals lying at the Fermi surface. In comparison to shell-model calculations, the high measured inclusive cross sections hint at significant bound $f_{7/2}$ neutron strength, which is outside the shell-model space considered here. In contrast, the relative single-particle strength distribution for the knockout to ^{69}Ni is described well by the shell model calculations if we consider the tentative ^{69}Ni level scheme proposed here. The results for the neutron removal to ^{67}Ni challenge the validity of one of the most current shell-model Hamiltonians, highlighting its shortcomings and providing benchmarks for future interactions developed for this neutron-rich region of the nuclear chart. The results suggest that our understanding of the low-energy states in these interesting nuclei is not yet complete and requires further investigation.

[1] S. Suchyta, S. N. Liddick, Y. Tsunoda, T. Otsuka, M. B. Bennett, A. Chemey, M. Honma, N. Larson, C. J. Prokop, S. J. Quinn, et al., Phys. Rev. C **89**, 021301 (2014).

[2] Y. Tsunoda, T. Otsuka, N. Shimizu, M. Honma, and Y. Utsuno, Phys. Rev. C **89**, 031301 (2014).

[3] A. Gade and S. N. Liddick, J. Phys. G **43**, 024001 (2016).

[4] T. Otsuka, R. Fujimoto, Y. Utsuno, B. A. Brown, M. Honma, and T. Mizusaki, Phys. Rev. Lett. **87**, 082502 (2001).

[5] T. Otsuka, T. Suzuki, R. Fujimoto, H. Grawe, and Y. Akaishi, Phys. Rev. Lett. **95**, 232502 (2005).

[6] T. Otsuka, T. Suzuki, M. Honma, Y. Utsuno, N. Tsunoda, K. Tsukiyama, and M. Hjorth-Jensen, Phys. Rev. Lett. **104**, 012501 (2010).

[7] O. Sorlin and M.-G. Porquet, Prog. in Part. Nucl. Phys. **61**, 602 (2008).

[8] A. Gade, Eur. Phys. J. A **51**, 1 (2015).

[9] A. Poves, J. of Phys. G: Nuclear and Particle Physics **43**, 024010 (2016).

[10] P. T. Hosmer, H. Schatz, A. Aprahamian, O. Arndt, R. R. C. Clement, A. Estrade, K.-L. Kratz, S. N. Liddick, P. F. Mantica, W. F. Mueller, et al., Phys. Rev. Lett. **94**, 112501 (2005).

[11] F. Recchia, C. J. Chiara, R. V. F. Janssens, D. Weisshaar, A. Gade, W. B. Walters, M. Albers, M. Alcorta, V. M. Bader, T. Baugher, et al., Phys. Rev. C **88**, 041302 (2013).

[12] C. J. Chiara, R. Broda, W. B. Walters, R. V. F. Janssens, M. Albers, M. Alcorta, P. F. Bertone, M. P. Carpenter, C. R. Hoffman, T. Lauritsen, et al., Phys. Rev. C **86**, 041304 (2012).

[13] S. M. Lenzi, F. Nowacki, A. Poves, and K. Sieja, Phys. Rev. C **82**, 054301 (2010).

[14] A. Gade, R. V. F. Janssens, T. Baugher, D. Bazin, B. A. Brown, M. P. Carpenter, C. J. Chiara, A. N. Deacon, S. J. Freeman, G. F. Grinyer, et al., Phys. Rev. C **81**, 051304 (2010).

[15] H. L. Crawford, R. M. Clark, P. Fallon, A. O. Macchiavelli, T. Baugher, D. Bazin, C. W. Beausang, J. S. Berryman, D. L. Bleuel, C. M. Campbell, et al., Phys. Rev. Lett. **110**, 242701 (2013).

[16] T. Braunroth, A. Dewald, H. Iwasaki, S. M. Lenzi, M. Albers, V. M. Bader, T. Baugher, T. Baumann, D. Bazin, J. S. Berryman, et al., Phys. Rev. C **92**, 034306 (2015).

[17] T. Baugher, A. Gade, R. V. F. Janssens, S. M. Lenzi, D. Bazin, B. A. Brown, M. P. Carpenter, A. N. Deacon, S. J. Freeman, T. Glasmacher, et al., Phys. Rev. C **86**, 011305 (2012).

[18] M. P. Carpenter, R. V. F. Janssens, and S. Zhu, Phys. Rev. C **87**, 041305 (2013).

[19] A. Dijon, E. Clément, G. de France, G. de Angelis, G. Duchêne, J. Dudouet, S. Franchoo, A. Gadea, A. Gottardo, T. Hüyük, et al., Phys. Rev. C **85**, 031301 (2012).

[20] S. Zhu, R. V. F. Janssens, M. P. Carpenter, C. J. Chiara, R. Broda, B. Fornal, N. Hoteling, W. Królas, T. Lauritsen, T. Pawłat, et al., Phys. Rev. C **85**, 034336 (2012).

[21] R. Broda, T. Pawłat, W. Królas, R. V. F. Janssens, S. Zhu, W. B. Walters, B. Fornal, C. J. Chiara, M. P. Carpenter, N. Hoteling, et al., Phys. Rev. C **86**, 064312 (2012).

[22] F. Flavigny, D. Pauwels, D. Radulov, I. J. Darby, H. De Witte, J. Diriken, D. V. Fedorov, V. N. Fedosseev, L. M. Fraile, M. Huyse, et al., Phys. Rev. C **91**, 034310 (2015).

[23] C. J. Chiara, D. Weisshaar, R. V. F. Janssens, Y. Tsunoda, T. Otsuka, J. L. Harker, W. B. Walters, F. Recchia, M. Albers, M. Alcorta, et al., Phys. Rev. C **91**, 044309 (2015).

[24] C. J. Prokop, B. P. Crider, S. N. Liddick, A. D. Ayangeakaa, M. P. Carpenter, J. J. Carroll, J. Chen, C. J. Chiara, H. M. David, A. C. Dombos, et al., Phys. Rev. C **92**, 061302 (2015).

[25] J. Diriken, N. Patronis, A. Andreyev, S. Antalic, V. Bildstein, A. Blazhev, I. Darby, H. D. Witte, J. Eberth, J. Elseviers, et al., Phys. Lett. B **736**, 533 (2014).

[26] A. Gade and T. Glasmacher, Prog. Part. Nucl. Phys. **60**, 161 (2008).

[27] A. Gade and B. M. Sherrill, Phys. Scrip. **91**, 053003 (2016).

[28] D. Morrissey, B. Sherrill, M. Steiner, A. Stolz, and I. Wiedenhoever, Nucl. Instrum. Methods in Phys. Res. Sect. B **204**, 90 (2003).

[29] S. Paschalis, I. Lee, A. Macchiavelli, C. Campbell, M. Cromaz, S. Gros, J. Pavan, J. Qian, R. Clark, H. Crawford, et al., Nucl. Instrum. Methods in Phys. Res. Sect. A **709**, 44 (2013).

[30] D. Bazin, J. Caggiano, B. Sherrill, J. Yurkon, and A. Zeller, Nucl. Instrum. Methods in Phys. Res. Sect. B **204**, 629 (2003).

[31] H. Mach, M. Lewitowicz, M. Stanoiu, F. Becker, J. Blomqvist, M. Berge, R. Boutami, B. Cederwall, Z. Dlouhy, B. Fogelberg, et al., Nucl. Phys. A **719**, C213 (2003).

[32] K. Meierbachtol, D. Bazin, and D. Morrissey, Nucl. Instrum. Methods in Phys. Res. Sect. A **652**, 668 (2011).

[33] K. Wimmer, D. Barofsky, D. Bazin, L. Fraile, J. Lloyd, J. Tompkins, and S. Williams, Nucl. Instrum. Methods in Phys. Res. Sect. A **769**, 65 (2015).

[34] E. Farnea, F. Recchia, D. Bazzacco, T. Kröll, Z. Podolyak, B. Quintana, and A. Gadea, Nucl. Instrum. Methods in Phys. Res. Sect. A **621**, 331 (2010).

[35] L. A. Riley, Ursinus College, UCGretina GEANT4, unpublished.

[36] J. A. Tostevin and A. Gade, Phys. Rev. C **90**, 057602 (2014).

[37] See Supplemental Material at http://link.aps.org/supplemental/10.1103/yyy.zz.xxxxxx for full details of the reaction model parameters, shell-model spectroscopy, and calculated cross sections.

[38] P. Hansen and J. Tostevin, Annu. Rev. Nucl. Part. Sci. **53**, 219 (2003).

[39] S. R. Stroberg, A. Gade, J. A. Tostevin, V. M. Bader, T. Baugher, D. Bazin, J. S. Berryman, B. A. Brown, C. M. Campbell, K. W. Kemper, et al., Phys. Rev. C **90**, 034301 (2014).

[40] A. E. L. Dieperink and T. d. Forest, Phys. Rev. C **10**, 543 (1974).

[41] C. Bertulani and A. Gade, Comp. Phys. Comm. **175**, 372 (2006).

[42] J. Diriken, N. Patronis, A. Andreyev, S. Antalic, V. Bildstein, A. Blazhev, I. G. Darby, H. De Witte, J. Eberth,

J. Elseviers, et al., Phys. Rev. C **91**, 054321 (2015).

[43] R. Grzywacz, R. Béraud, C. Borcea, A. Emsallem, M. Glogowski, H. Grawe, D. Guillemaud-Mueller, M. Hjorth-Jensen, M. Houry, M. Lewitowicz, et al., Phys. Rev. Lett. **81**, 766 (1998).

[44] W. F. Mueller, B. Bruyneel, S. Franchoo, H. Grawe, M. Huyse, U. Köster, K.-L. Kratz, K. Kruglov, Y. Kudryavtsev, B. Pfeiffer, et al., Phys. Rev. Lett. **83**, 3613 (1999).

[45] S. N. Liddick, W. B. Walters, C. J. Chiara, R. V. F. Janssens, B. Abromeit, A. Ayres, A. Bey, C. R. Bingham, M. P. Carpenter, L. Cartegni, et al., Phys. Rev. C **92**, 024319 (2015).

[46] M. Moukaddam, Evolution of the shell structure in medium-mass nuclei : Search for the $2d_{5/2}$ neutron orbital in ^{69}Ni. PhD Thesis, Universite de Strasbourg (2012).

[47] B. A. Brown, W. D. M. Rae, E. McDonald, and M. Horoi, NuShellX@MSU, B. A. Brown, W. D. M. Rae, E. McDonald, and M. Horoi, http://www.nscl.msu.edu/brown/resources/resources.html; NuShellX, W. D. M. Rae, http://www.garsington.eclipse.co.uk/.

[48] A. F. Lisetskiy, B. A. Brown, M. Horoi, and H. Grawe, Phys. Rev. C **70**, 044314 (2004).

[49] B. A. Brown, unpublished.

[50] M. Honma, T. Otsuka, T. Mizusaki, and M. Hjorth-Jensen, Phys. Rev. C **80**, 064323 (2009).